Electronic Supplementary Material (ESI) for Polymer Chemistry.


**Electronic Supplementary Information**

# The Influence of Depropagation on $PEGMA_9$ Solution Radical Homopolymerization and Copolymerization with DEAEMA: *in situ* $^1$H-NMR Measurements and Reactivity Ratios Estimation by Dynamic Optimization

*Judith Cabello-Romero,[1] Román Torres-Lubián,[1] Francisco Javier Enríquez-Medrano,[1] Robin A. Hutchinson,[2,*] Iván Zapata-González[3,*]*

**AUTHOR ADDRESS**

1. Dpto. de Química Macromolecular y Nanomateriales, Centro de Investigación en Química Aplicada (CIQA), #140, Blvd. Enrique Reyna Hermosillo, Saltillo, 25294, Coahuila, México.
2. Dept. of Chemical Engineering, Dupuis Hall, Queen's University, Kingston, Ontario K7L 3N6, Canada
3. Dpto. de Procesos de Polimerización, Centro de Investigación en Química Aplicada (CIQA), #140, Blvd. Enrique Reyna Hermosillo, Saltillo, 25294, Coahuila, México.

## 1. Derivation of the Models

### 1.1. Dynamic Mayo Lewis (DML) model[1]

This model was previously reported by Guerrero-Sanchez et al. for a radical copolymerization system in batch and continues stirrer tank reactors, here we resume the derivation.

Defining the overall molar conversion of the copolymerization system

$$\boldsymbol{X}= \frac{\left([M_1]_0+[M_2]_0\right)-\left([M_1]+[M_2]\right)}{\left([M_1]_0+[M_2]_0\right)} \tag{S1}$$

Taking the derivative of Eqn. (S1) regarding time results in

$$\frac{d\boldsymbol{X}}{dt}=-\frac{1}{[M_1]_0+[M_2]_0}\left(\frac{d[M_1]}{dt}+\frac{d[M_2]}{dt}\right) \tag{S2}$$

Using the chain rule for the derivatives, the inverse function theorem, we obtain Eqn. (S3)

$$\frac{d[M_1]}{d\boldsymbol{X}}=\frac{1}{\frac{d\boldsymbol{X}}{dt}}\left(\frac{d[M_1]}{dt}\right)=-\frac{\left([M_1]_0+[M_2]_0\right)}{1+\left(\frac{d[M_2]}{d[M_1]}\right)} \tag{S3}$$

The Mayo Lewis equation for the term $\left(\frac{d[M_2]}{d[M_1]}\right)$ is given by

$$\frac{d\left[M_2\right]}{d\left[M_1\right]}=\left(\frac{\left[M_2\right]}{\left[M_1\right]}\right)\frac{\left[M_1\right]+r_2\left[M_2\right]}{\left[M_2\right]+r_1\left[M_1\right]} \tag{S4}$$

Substituting the Eqn. (S4) in Eqn. (3) results Eqn. (9)

$$\frac{d[M_1]}{dX} = -\frac{\left([M_1]_0 + [M_2]_0\right)}{1+\left(\left(\frac{[M_2]}{[M_1]}\right)\frac{[M_1]+r_2[M_2]}{[M_2]+r_1[M_1]}\right)} \tag{9}$$

Analogously following the same procedure for the $M_2$ material balance, we found:

$$\frac{d[M_2]}{dX} = -\frac{\left([M_1]_0 + [M_2]_0\right)}{1+\left(\left(\frac{[M_1]}{[M_2]}\right)\frac{[M_2]+r_1[M_1]}{[M_1]+r_2[M_2]}\right)} \tag{10}$$

### 1.2. Lowry Case 1 (LC1) and Lowry Case 3 (LC2) Models

Eqn. (S3) is used for the derivation of the LC1 and LC2 models, therefore Eqn. (9) and (10) are substituted in Eqn. (S3) giving Eqn. (28) and Eq. (30), respectively.

$$\frac{d[M_1]}{dX} = -\frac{\left([M_1]_0 + [M_2]_0\right)}{1+\left(\frac{[M_2]\left(1/(1-\alpha)\right)}{r_1[M_1]+[M_2]}\right)} \tag{28}$$

$$\frac{d[M_1]}{dX} = -\frac{\left([M_1]_0 + [M_2]_0\right)}{1+\left(\frac{\alpha\gamma - 1 + \left(1/(1-\alpha)\right)^2}{\left\{\left(r_1[M_1]/[M_2]\right)+1\right\}+\left\{\alpha\gamma - 1 + \left(1/(1-\alpha)\right)\right\}}\right)} \tag{30}$$

## 2. Stacked $^{1}$H-NMR spectra

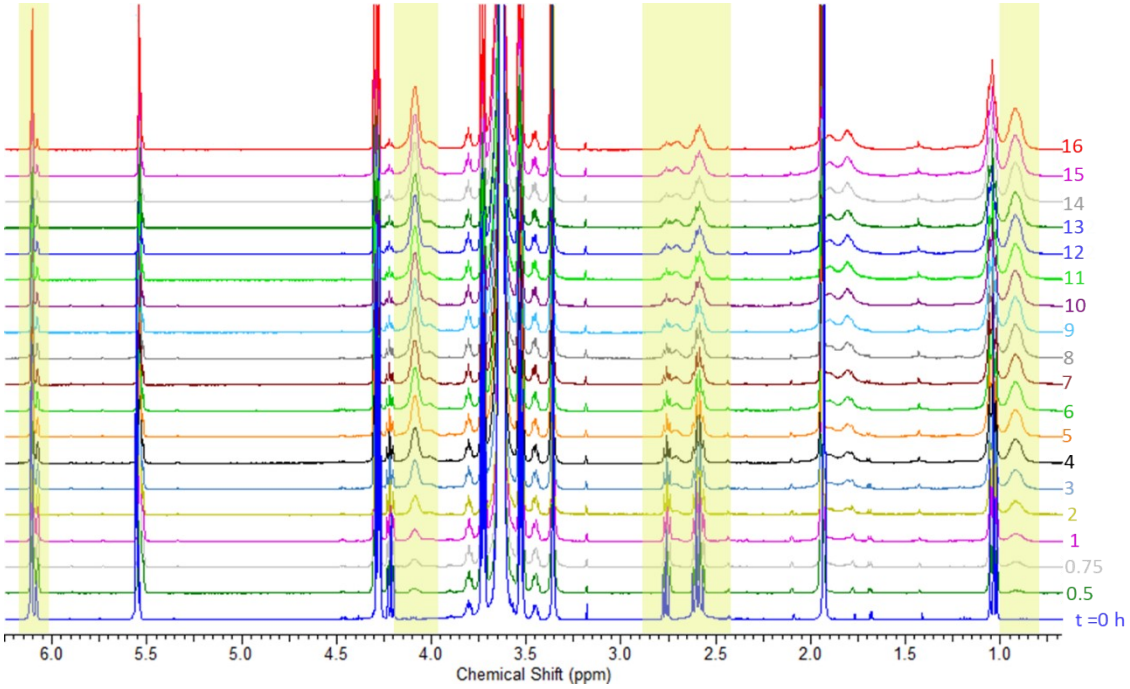


**Figure 1S.** Stacked $^{1}$H-NMR spectra at intervals of 60 min (bottom to top) for the copolymerization DEAEMA and $PEGMA_9$ with an initial 14:86 molar ratio in $CDCl_3$ at 65°C**.**

### 3. Individual monomer conversion *versus* time

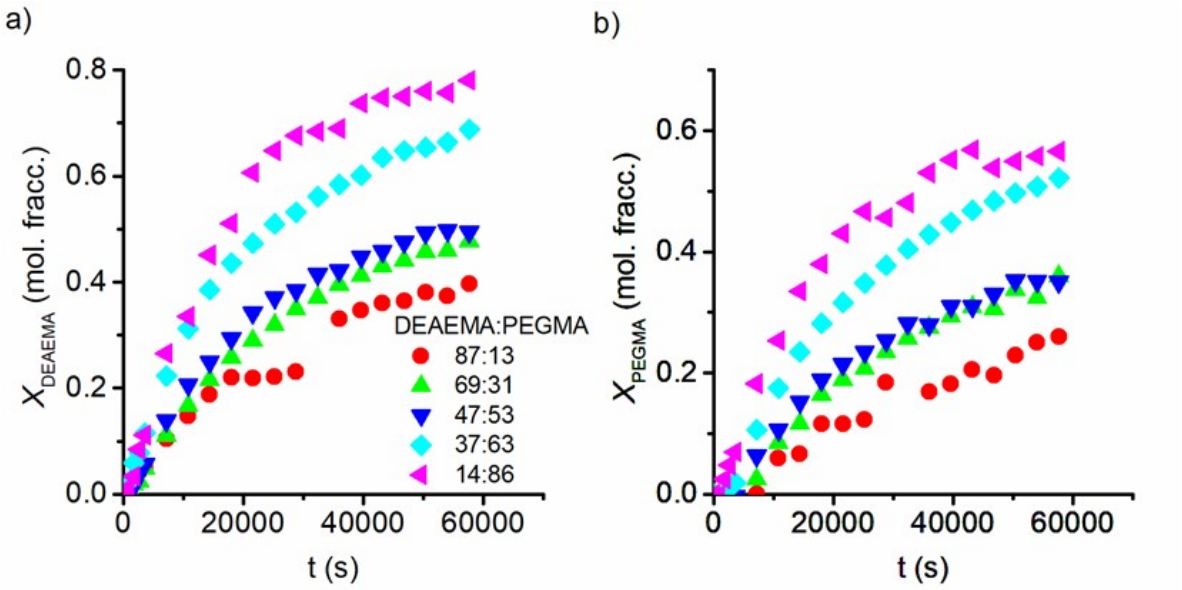


**Figure 2S.** Plot of the individual monomer conversion *versus* time using AIBN in CDCl3 at 65 °C: a) $X_{DEAEMA}$ *versus* time and b) $X_{PEGMA9}$ *versus* time. The labels indicate the initial monomer composition of DEAEMA: PEGMA (mol%: mol%).

## 4. Viscosity of the polyPEGMA solution

We carried out $PEGMA_9$ polymerizations using $CDCl_3$ and AIBN at 65 °C, using two PEGMA concentrations. For instance, a stock solution of $PEGMA_9$ (0.31 g), AIBN (0.0004 g) and $CDCl_3$ (5.55 g) (173 mM) was prepared. An aliquot of ~2 g was transferred to an ignition tube, degassed with three freeze-evacuate-thaw cycles, and sealed. The tube was then heated to 65 °C in an oil bath and left for 24 hours. The reaction mixture was analyzed by $^1H$ NMR to calculate monomer conversion and the viscosity was measured in an Anton Paar rheometer MCR 501 at 25 °C, using a geometry CP25-1-SN23404; d=0.049 mm. A similar procedure was carried out to prepare, polymerize and characterize a solution with $[PEGMA]_0$ = 370 mM. Results indicate a much higher value of zero-shear viscosity ($\eta_o$) for the polymerization with $[PEGMA]_0$ = 370 mM, reaching 28.76 Pa s, than that for $PEGMA]_0$ = 173 mM (0.015 Pa s), see Figure 3S. This behavior is consistent with the hypothesis that PEG side chains are entangled, resulting in a mild Trommsdorf effect, which is the origin of the liner deviations in Figure 5c, as mentioned in the main.

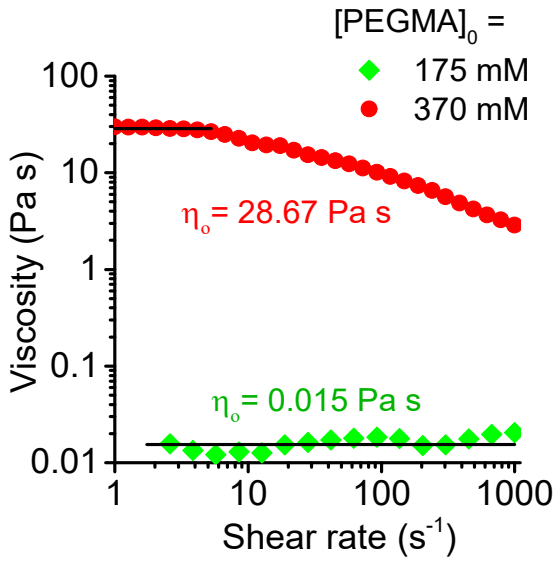


**Figure. 3S** Viscosity curves with estimated values of zero-shear viscosity ($\eta_o$)

## 5. $PEGMA_9$ homopolymerization rates

Linear regressions for Eqn. (21) are plotted in **Figure 5d** for $PEGMA_9$ polymerization data, wherein the slops represent the apparent kinetic coefficient $k_p/k_t^{0.5}$ for short times Surprisingly, the value of $k_p/k_t^{0.5}$ is increased at higher $[PEGMA_9]_0$, see AIBN 1 *versus* AIBN 2 and AIBN 3. If $k_p$ remains constant during the copolymerizations, as previous studies have reported for linear polymerizations,[1] the decrease in the value of $\langle k_t \rangle$ for experiment AIBN 2 and AIBN 3 regarding to experiment AIBN 1 are 1.84 and 7.86 times. It is clear that PEG side chains do not present intermolecular interactions with the $CDCl_3$; thus, the high value of $k_t$ cannot attributed to this factor. Instead, the conformation of the bottlebrush becomes an important hypothesis, as explained in the main text.

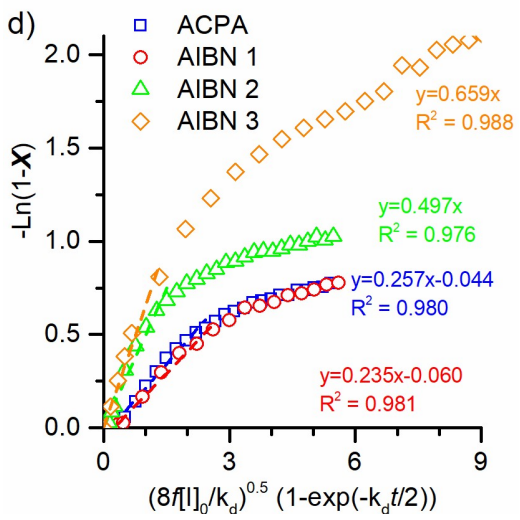


**Figure 4S.** Linear fitting of Eqn.(15) for polymerization of $PEGMA_9$ in CDCl3 at 65 °C using ACPA and AIBN, dashed lines are linear regressions.

(1) Buback, M. Free-radical Propagation Rate Coefficients. *Can. J. Chem. Eng.* 2023, 1. https://doi.org/10.1002/cjce.24885

## 6. Monomer and Copolymer composition profiles using r's estimated by NLLS model.

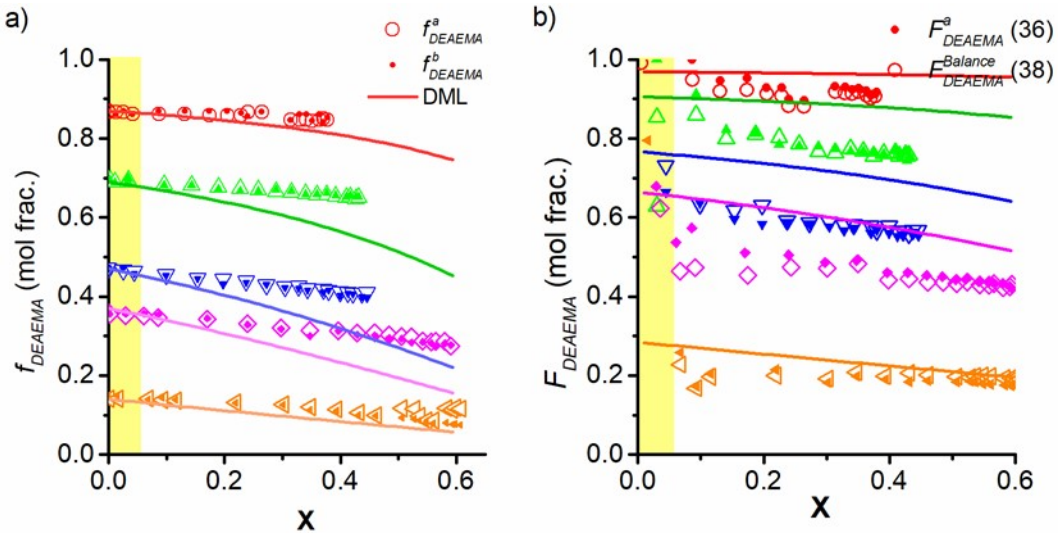


**Figure 5S.** Comparison between the experimental data (symbols) and the theory profiles (lines) using the estimated values by NLLS model at only low conversion data (yellow region): a) compositional drift of the remaining monomer mixture and b) compositional drift of the copolymer composition. The *r* values are presented in **Table 3**.

## 7. Monomer and Copolymer composition profiles using r's estimated by DML (f) and DML (F) models.

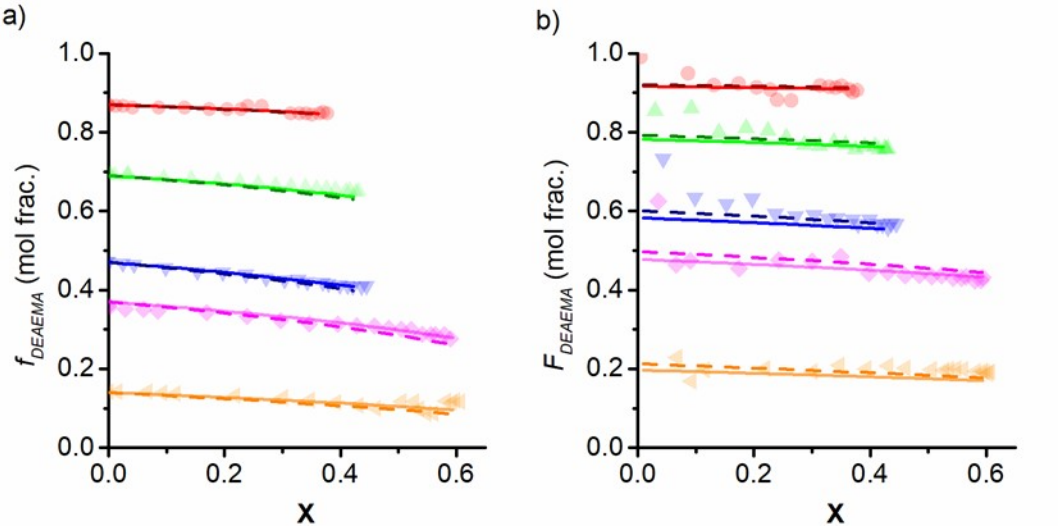


**Figure 6S.** Comparison between the experimental data (symbols), model DML (f) (dashed lines) and model DMF (F) (solid lines) in: a) Compositional drift of the remaining monomer mixture (Eq. 34) and b) Compositional drift of the copolymer composition (Eq. 36). The r values are presented in **Table 3.**

8. **Monomer and Copolymer composition profiles using r's estimated by LC1 (f) 3 var. and LC2 (f) 3 var. models.**

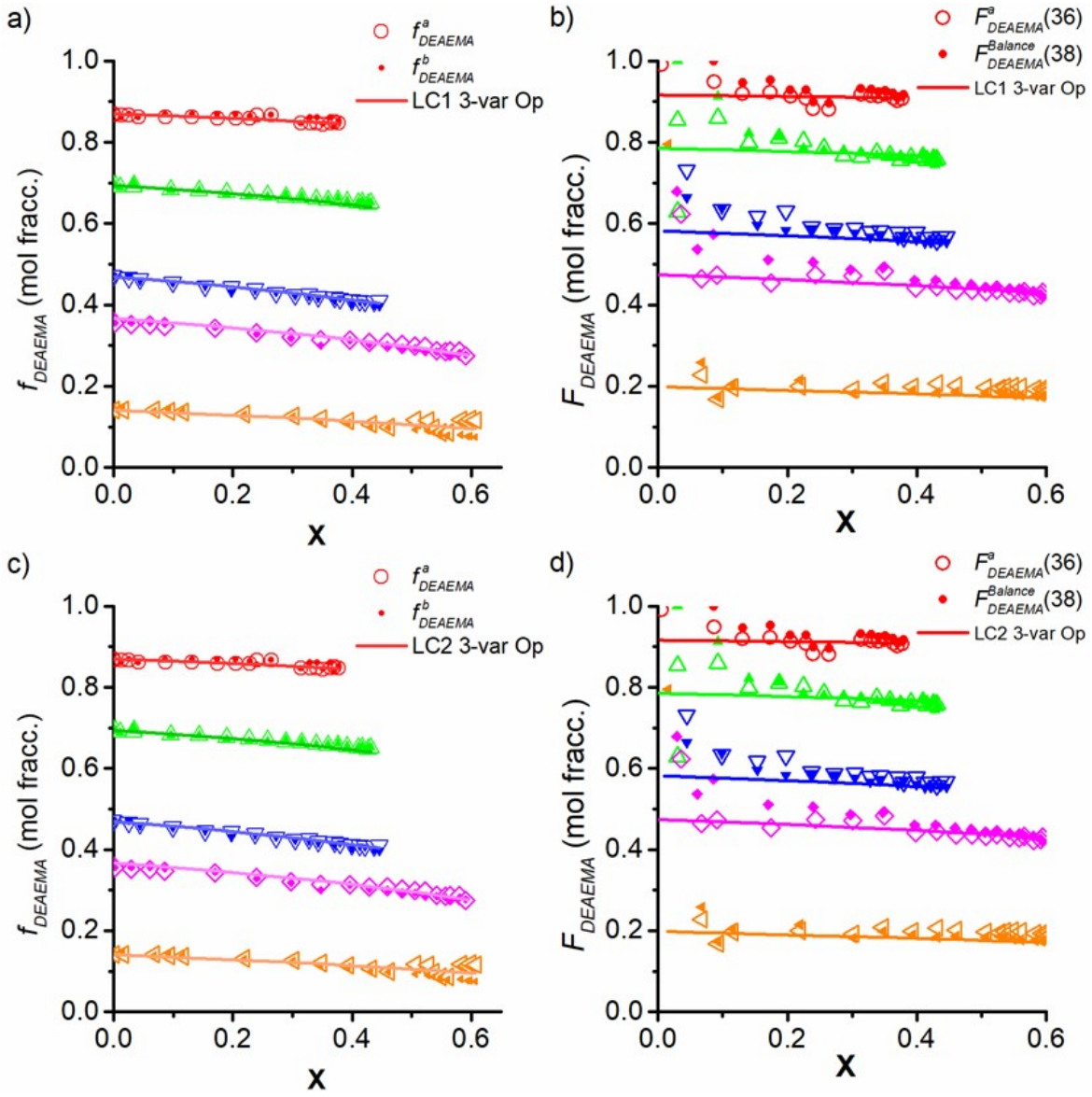


**Figure 7S.** Comparison of dynamic models (lines) using three-variable optimization algorithm and experimental (symbols) batch composition drifts for DEAEMA copolymerized with $PEGMA_9$ at 65°C using AIBN, with varying initial comonomer compositions. a) and b) LC1 model, c) and d) LC2 model. The two values of $f_{DEAEMA}$ in a), c) and e) are estimated from NMR integrations according to Eqn. (34) and (35), while the two $F_{DEAEMA}$ estimates in b), d)

and f) are from NMR integrations (Eqn. 36) and mass balances (Eqn. 38). The values of r and $K_{eq}$ are presented in Table 3.